ESC HEART FAILURE
ESC Heart Failure 2022; **9**: 1050–1060
Published online 30 December 2021 in Wiley Online Library (wileyonlinelibrary.com) **DOI:** 10.1002/ehf2.13766

ORIGINAL ARTICLE

Knockdown of XIST up-regulates 263294miR-340-5p to relieve myocardial ischaemia–reperfusion injury via inhibiting cyclin D1

Qijun Bai[1], Yan Li[1], Kunpeng Song[1]*, Jie Huang[2] and Li Qin[1]

[1]*Department of Cardiovascular Medicine Ward II, Zhengzhou Central Hospital Affiliated to Zhengzhou University, 16 North Tongbai Road, Zhongyuan District, Zhengzhou, Henan 450000, China; and* [2]*Department of Geriatric Medicine, Zhengzhou Central Hospital, Zhengzhou, Henan, China*

Abstract

Aim Long non-coding RNAs (lncRNAs) are known to participate in various human diseases, while the role of X inactive-specific transcript (XIST) binding microRNA-340-5p (miR-340-5p) remains seldom studied. We aim to identify the role of the XIST/miR-340-5p/cyclin D1 (CCND1) axis in the myocardial ischaemia–reperfusion injury (MIRI).

Methods and results The mouse MIRI models were established. The expression of XIST, miR-340-5p, and CCND1 in mouse myocardial tissues in MIRI mice was assessed. The MIRI mice were respectively treated with altered XIST, miR-340-5p, or CCND1. The changes of myocardial enzyme activity were assessed, and the cardiac function was evaluated. Myocardial pathological changes, cardiomyocyte apoptosis and related apoptotic factors, oxidative stress and inflammatory factors were observed in myocardial tissues in mice with MIRI. The binding relationships between XIST and miR-340-5p, and between miR-340-5p and CCND1 were confirmed. XIST and CCND1 were up-regulated while miR-340-5p was down-regulated in MIRI mice. Silenced XIST could elevated miR-340-5p expression and reduced CCND1 expression, so as to promoted cardiac function and suppressed myocardial enzyme activity, ameliorated pathological changes, decelerated cardiomyocyte apoptosis by elevating Bcl-2 but reducing the levels of Bax and Caspase-3, attenuated inflammatory response by repressing IL-6 and TNF-α levels, and mitigated oxidative stress by reducing MDA contents and increasing CAT, GSH-Px, and SOD levels in MIRI mice. XIST sponged miR-340-5p and miR-340-5p targeted CCND1.

Conclusions Knockdown of XIST up-regulates miR-340-5p to relieve MIRI via inhibiting CCND1.

Keywords Myocardial ischaemia–reperfusion injury; Long non-coding RNA X inactive-specific transcript; MicroRNA-340-5p; Cyclin D1; Cardiomyocyte

Received: 24 May 2021; Revised: 24 November 2021; Accepted: 2 December 2021
**Correspondence to: Dr Kunpeng Song, Department of Cardiovascular Medicine Ward II, Zhengzhou Central Hospital Affiliated to Zhengzhou University, 16 North Tongbai Road, Zhongyuan District, Zhengzhou 450000, Henan Province, China. Tel: +86-0371-67690959. Email: Songkunpeng195@163.com*

Introduction

Coronary artery disease (CAD), a main cause for morbidity and mortality throughout the world, is a common health problem.[1] The most common form of CAD is atherosclerosis. With the forming of lipid-rich plaques, atherosclerosis can gradually obstruct the vessel lumen, leading to coronary occlusion and cessation of blood flow.[2] Restoration of blood flow to ischaemic myocardium is usually used to treat ischaemic heart disease. Restoring blood flow minimizes infarct-induced damage, thereby decreasing the mortality. Nevertheless, this restoration may lead to additional cardiovascular trauma, namely, myocardial ischaemia–reperfusion (I/R) injury (MIRI).[3] MIRI can result in cell death and cardiac dysfunction, and its potential mechanisms involve in oxidative stress, calcium overload, inflammation, neutrophil infiltration, and cytokine release.[4] Although the treatments for this disease, such as percutaneous coronary intervention technology, antiplatelet agent, and antithrombotic agent, have been developed, there is still no effective therapeutic strategy to fight against MIRI.[5] Therefore, it is necessary to explore novel therapeutic targets for MIRI.

Long non-coding RNA (lncRNA) is a group of functional RNA molecule with transcript length of >200 nt and is implicated in multiple physiological and pathological processes.[6] Some particular lncRNAs were involved in MIRI. For instance, lncRNA RMRP up-regulation has been reported to aggravate MIRI,[7] and it has been identified that knockdown of lncRNA AK139328 alleviated MIRI.[8] LncRNA X inactive-specific transcript (XIST) is a major regulator of mammalian X chromosome inactivation,[9] which has been demonstrated to regulate myocardial infarction (MI)[10] and hypoxia-induced cardiomyocyte apoptosis.[11] Interestingly, the reduction of XIST has been verified to improve MIRI.[12] In recent decades, the competing endogenous RNA (ceRNA) hypothesis implies a regulatory circuitry that lncRNAs can serve as molecular sponges of specific microRNAs (miRNAs).[13] MiRNAs are small non-protein-coding RNAs that regulate gene expression by binding to the 3′-untranslated region (3′-UTR) of mRNAs and promoting degradation of transcripts or inhibiting translation.[14] As one of the miRNAs, miR-340-5p has been clarified to inhibit hypoxia/reoxygenation (H/R)-induced apoptosis and oxidative stress in cardiomyocytes.[15] However, the spongy relationship between XIST and miR-340-5p remains largely unknown. Cyclin D1 (CCND1) is a highly conserved cyclin family protein that has been identified as the indispensable for the transition of cell cycle from G1 phase into S phase.[16] As reported, CCND1 was implicated in hypoxia-induced myocardial damage,[17] and it has been elucidated that there exists a targeting relationship between miR-340-5p and CCND1 in multiple myeloma.[18] However, this relationship in MIRI remains scarcely studied.

Thus, we aimed to explore the role of the XIST/miR-340-5p/CCND1 axis during the MIRI, and we inferred that XIST may act as a ceRNA of miR-340-5p to affect MIRI through targeting CCND1.

Materials and methods

Ethics statement

Animal experiments were strictly in accordance with the Guide to the Management and Use of Laboratory Animals issued by the National Institutes of Health. The protocol of animal experiments was approved by the Institutional Animal Care and Use Committee of Zhengzhou Central Hospital.

Experimental animals

Adult male-specific pathogen-free mice aged 10–12 weeks (the experimental animal centre of Zhengzhou University, Henan, China) were fed at 25°C and with 50% humidity.

Animal grouping

XIST shRNA, miR-340-5p antagomir, CCND1 shRNA, or the negative control (NC) were added to lentiviral vectors PHY-LV-KD5.1 (Thermo Fisher Scientific Inc., MA, USA) and then were packaged into lentiviral particles. Mouse left ventricle was injected with 200 μL lentivirus (1×10^9 TU/mL). The pulmonary artery was clamped for 20 s to maintain heartbeat in a closed system. Then, the air and blood were removed and the incision was sutured.[19]

Mice were classified into eight groups (n = 12): the sham, ischaemia–reperfusion (I/R), NC, sh-XIST, sh-CCND1, antagomir NC, miR-340-5p antagomir, and si-XIST + miR-340-5p antagomir groups.[19]

Establishment of ischaemia–reperfusion mouse models

Mice were modelled 5 days after lentivirus injection: mice were anaesthetized by 1% pentobarbital sodium (35 mg/kg, Qiaoxing Trading Co., Ltd., Shanghai, China). The left thoracic cavity was opened with a surgical scalpel, and the left anterior descending coronary artery (LAD) was ligated by 10-0 nylon suture to induce ischaemia for 30 min, then the suture was loosen for 60 min of reperfusion. After the I/R procedure, the chest was closed and the endotracheal intubation was removed. The sham group underwent the same surgery except the LAD ligation. After euthanasia, the blood and myocardial tissues were harvested.[19]

Color Doppler echocardiography

Mice were intraperitoneally injected with 1% pentobarbital sodium (35 mg/kg) 48 h after reperfusion and then were fixed at a supine position to measure the left ventricular end-diastolic diameter (LVEDD), end-systolic dimension (LVESD), ejection fraction (LVEF), fractional shortening (LVFS), systolic pressure (LVSP), and end-diastolic pressure (LVEDP) by ultrasound Doppler examination.[20]

Detection of serum myocardial enzyme levels

The determination of myocardial enzyme levels during MIRI has some intrinsic significance compared with the intuitive nature of microscopic analysis of myocardial sections.[21,22] Myocardial enzyme is a general term for a variety of enzymes present in the myocardium, including aspartate aminotransferase, lactate dehydrogenase (LDH), creatine kinase (CK) and isoenzymes, and α-hydroxybutyrate dehydrogenase. The cardiac enzymes are released due to myocyte necrosis during MIRI, causing increased serum levels of cardiac en-

zymes. According to the instructions of relative cytotoxicity detection commercial kits (Jining Industrial Co., Ltd., Shanghai, China), the serum levels of LDH and CK were determined using spectrophotometry to measure the degree of myocardial ischaemia or cardiomyocyte apoptosis.

Haematoxylin–eosin staining

Mouse hearts were harvested and fixed in 4% paraformaldehyde and then were dehydrated, paraffin-embedded, sectioned, stained by haematoxylin and eosin (HE), and observed under a microscope.

Masson staining

The staining was conducted as previously described,[23] and the sections were observed under a microscope.

Terminal deoxynucleotidyl transferase-mediated deoxyuridine triphosphate nick end-labelling staining

The prepared myocardial sections were used to assess cardiomyocyte apoptosis using the terminal deoxynucleotidyl transferase-mediated deoxyuridine triphosphate nick end-labelling (TUNEL) kits. A light microscope was used for observation, and TUNEL positive cells were counted.[24]

Biochemical detection

Mouse myocardial tissues were made into homogenate, which was centrifuged at 3773 g for 15 min to produce the relative supernatant. The content of malondialdehyde (MDA) and activities of catalase (CAT), glutathione peroxidase (GSH-Px), and superoxide dismutase (SOD) were evaluated using relative detection kits.[25]

Reverse transcription quantitative polymerase chain reaction

Total RNA in tissues was extracted by TRIzol kits, purified using RNeasy mini kits (Qiagen, MA, USA), and cDNA was synthesized from total RNA by a PrimerScript RT Reagent kit (TaKaRa, Shiga, Japan). miRNA from total RNA was reverse transcribed using the Prime-Script miRNA cDNA Synthesis Kit (TaKaRa). Real-time (RT)-PCR was performed with the SYBR Green Premix Ex Taq II (TaKaRa), and data were analysed by $2^{-\Delta\Delta Ct}$ method with glyceraldehyde phosphate dehydrogenase (GAPDH) and U6 as the internal references. The primers were shown in Supporting Information.

Western blot analysis

Total protein was extracted from tissues, which was lysed by bicinchoninic acid kits and quantified. The proteins were transferred onto membranes and conducted with gel electrophoresis. The membranes were blocked for 1 h, incubated with primary antibodies CCND1 and GAPDH (all 1:500 and from Abcam Inc., MA, USA) at 4°C overnight, and incubated with relative secondary antibody for 2 h. The enhanced chemiluminescent reagent (Pierce, IL, USA) was used to analyse the membranes and the protein bands were observed.

Dual luciferase reporter gene assay

XIST and CCND1 3'untranslated region (3'UTR) sequences containing miR-340-5p binding site were synthesized and subcloned to pGL4 luciferase reporter vector (Promega, WI, USA), respectively, followed by construction of XIST and CCND1 3'UTR wild-type (WT) and mutation (MUT) plasmids. According to the manufacturer's information, HEK239 cells were co-transfected with constructed vectors together with NC or miR-340-5p mimic using Lipofectamine 3000 (Thermo Fisher) for 48 h. The luciferase activity was determined by dual luciferase reporter gene detection kits (Promega) and SpectraMax L (Molecular Devices, CA, USA).

RNA pull-down

HEK-293T cells were treated for 24 h with biotinylated miRNA (200 nM). Next, the cells were gently rinsed two times with PBS and then lysed for 10 min with ice-cold RNA pull-down lysis buffer on ice. The obtained lysate was centrifuged, and the supernatant that was aliquoted into 50 μL was used for subsequent input research. Afterward, streptavidin magnetic beads (Thermo Scientific Fisher) were supplemented to the remaining lysate, followed by incubation at room temperature and addition of RNase-free bovine serum albumin (Sigma) and yeast tRNA (Sigma). Subsequently, the mixture was incubated for 3 h at 4°C. The beads were rinsed with ice-cold lysis buffer and low-salt buffer for three times and lastly rinsed with high-salt buffer to obtain a pure sample. At last, TRIzol (Sigma) was adopted for purifying the bound RNAs, and RT-qPCR was carried out to analyze XIST expression.

Statistical analysis

All data analyses were conducted using SPSS 21.0 software (IBM Corp., Armonk, NY, USA). The data were expressed as mean ± standard deviation. The *t*-test was performed for comparisons between two groups, analysis of variance

(ANOVA) was used for comparisons among multiple groups, and Tukey's post hoc test was used for pairwise comparisons after ANOVA. P value < 0.05 was indicative of statistically significant difference.

Results

Ischaemia–reperfusion induces mouse myocardial tissue injury

Serum activities of LDH and CK were determined, and we found that I/R mice had higher LDH and CK activities than those in the sham group, indicating the formation of myocardial ischaemia (*Figure 1A*). Results of electrocardiogram suggested that LVEDD, LVESD, and LVEDP were increased while LVEF, LVFS, and LVSP were decreased in the I/R group versus the sham group (*Figure 1B–1D*). The HE staining showed that there were no characteristic pathological changes in mice of the sham group, while in the I/R group, there appeared congestion, haemorrhage, repairable inflammation, myocardial fibrosis, and even necrosis in mouse heart (*Figure 1E*). Moreover, in Masson staining, the normal cardiomyocytes were red while the fibrotic area was blue. We found that the blue area was nearly 0 in the sham group, while was increased in the I/R group (*Figure 1F*). TUNEL staining reflected that cardiomyocyte apoptosis was enhanced in I/R mice (*Figure*

Figure 1 I/R induces mouse myocardial tissue injury. (A) Detection of myocardial enzyme activity; (B–D) detection of haemodynamic indices; (E) representative images of HE staining; (F) representative images of Masson staining; (G) representative images of TUNEL staining; (H) mRNA expression of Bcl-2, Bax, and Caspase-3 assessed by RT-qPCR; (I–L) detection of oxidative stress-related factor levels; (M) levels of inflammatory factors; $n = 12$ in (A)–(D), $n = 6$ in (E)–(M); *$P < 0.05$ versus the sham group; the data were expressed as mean ± standard deviation, and the Student's t-test was performed for comparisons between two groups.

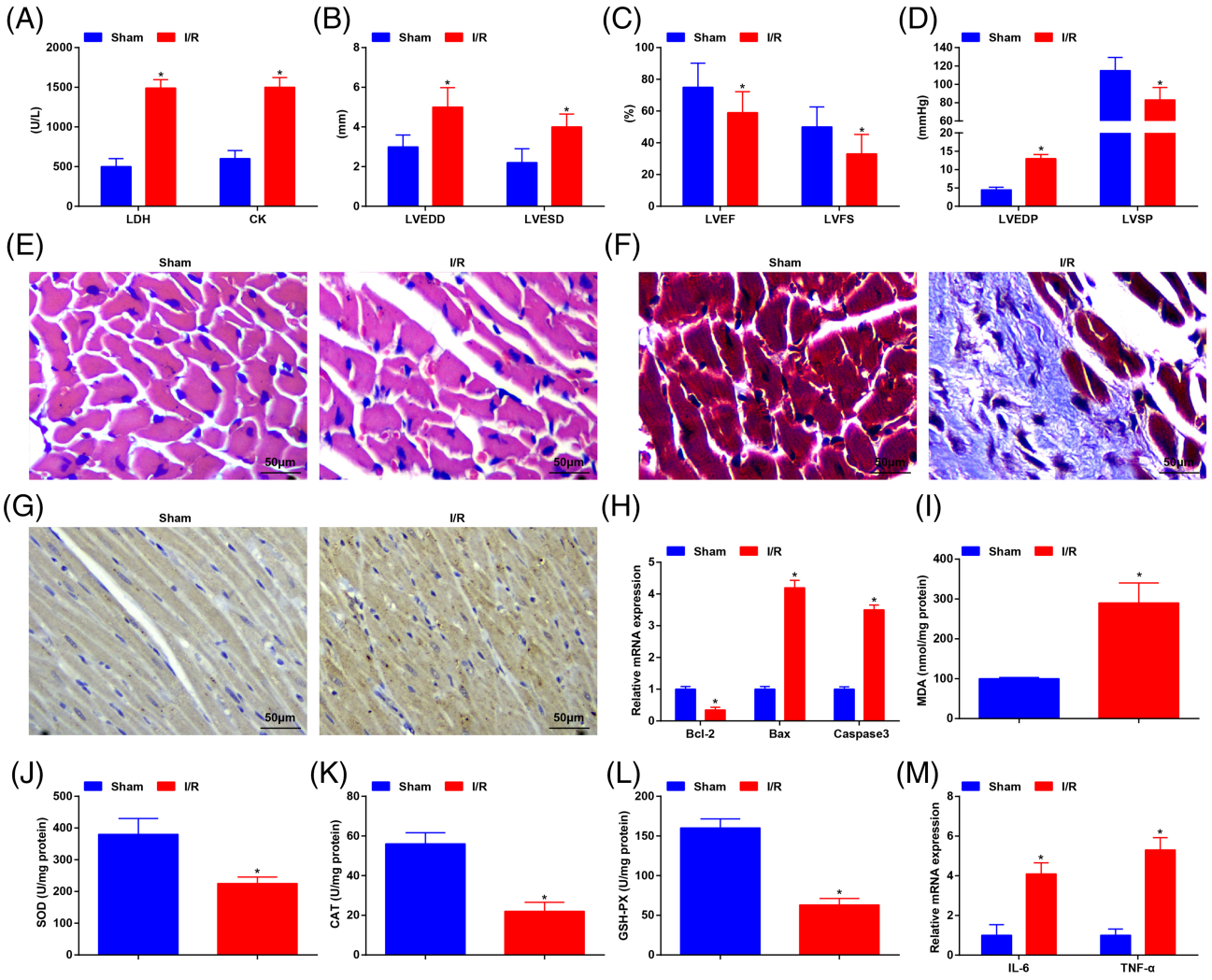

DOI: 10.1002/ehf2.13766

Figure 2 XIST knockdown relieves MIRI and cardiomyocyte apoptosis. (A/B) XIST expression in mice detected using RT-qPCR; (C) detection of myocardial enzyme activity; (D–F) detection of cardiac blood flow parameters; (G) representative images of HE staining; (H) representative images of Masson staining; (I) representative images of TUNEL staining; (J) mRNA expression of Bcl-2, Bax, and Caspase-3 assessed by RT-qPCR; (K–N) detection of oxidative stress-related factor levels; (O) levels of inflammatory factors; $n = 12$ in (C)–(F), $n = 6$ in (A) and (B), (G)–(O); $^{*}P < 0.05$ versus the sham group; $^{\#}P < 0.05$ versus the NC group; the data were expressed as mean ± standard deviation, and the *t*-test was performed for comparisons between two groups.

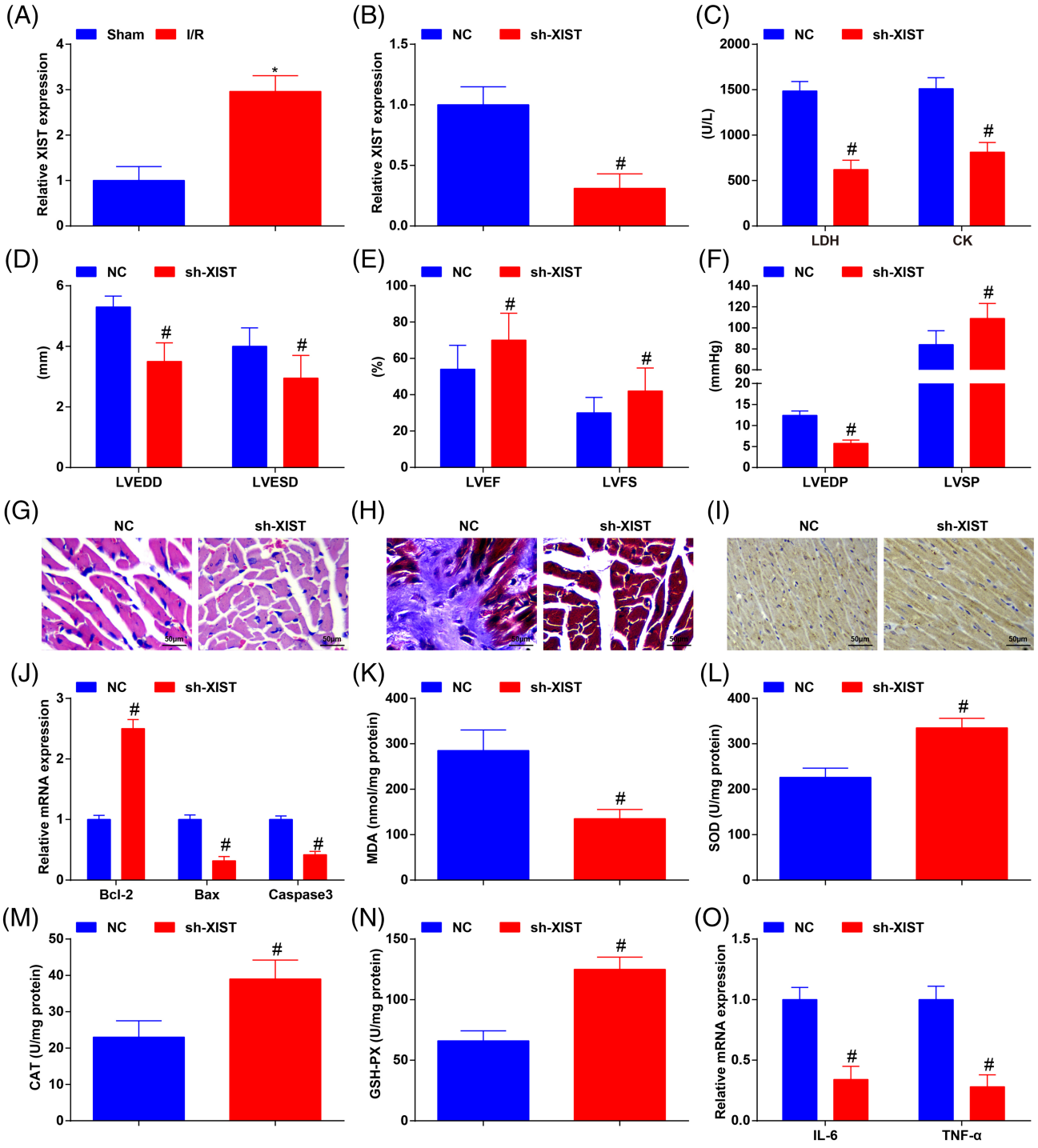

1G). The apoptosis-related markers were detected as well and it was revealed that I/R mice had decreased B-cell lymphoma-2 (Bcl-2) level and increased Bcl-2-associated X (Bax) and Caspase-3 levels, indicating increased apoptosis (*Figure 1H*). The levels of oxidative stress-related factors and inflammatory factors were determined and it was discovered that the levels of MDA, interleukin-6 (IL-6), and tumour necrosis factor-α (TNF-α) were increased whereas levels of SOD, CAT, and GSH-Px were decreased in I/R mice (*Figure 1I–1M*). The aforementioned findings implied that the I/R models were successfully established.

XIST knockdown relieves myocardial ischaemia–reperfusion injury and cardiomyocyte apoptosis

XIST expression in mouse myocardial tissues was detected and we found that it was overexpressed in I/R mice (*Figure 2A*). XIST was knocked down (*Figure 2B*) to observe its effect on MIRI, and results of our experiments indicated that XIST silencing suppressed myocardial enzyme activity, pathological changes, cardiomyocyte apoptosis, oxidative stress, and inflammatory response and promoted cardiac function in the I/R mice (*Figure 2C–2O*). These findings indicated that XIST knockdown relieved I/R-induced myocardial injury and cardiomyocyte apoptosis.

XIST targets miR-340-5p

It was predicated that there existed binding sites between XIST and miR-340-5p (*Figure 3A*), and it was further confirmed that the transfection of miR-340-5p mimic and XIST-WT suppressed the luciferase activity, which was not affected by transfection of miR-340-5p mimic and XIST-MUT (*Figure 3B*). Results of RNA pull-down assay indicated that XIST was enriched in the bio-miR-340-5p (*Figure 3C*), suggesting a direct binding relationship between XIST and miR-340-5p. Moreover, we found in RT-qPCR that miR-340-5p was down-regulated in I/R mice versus mice in the sham group, and miR-340-5p was up-regulated after XIST was knocked down (*Figure 3D* and *3E*). These data showed that XIST negatively regulated miR-340-5p expression.

MiR-340-5p reduction aggravates XIST-induced myocardial ischaemia–reperfusion injury

MiR-340-5p was down-regulated to observe its role in XIST-induced MIRI, and we also found that the dual knockdown of miR-340-5p and XIST restored miR-340-5p expression (*Figure 4A*). It was discovered through a series of assays that miR-340-5p down-regulation aggravated myocardial enzyme activity, pathological changes, cardiomyocyte apoptosis, oxidative stress, and inflammatory response and

Figure 3 XIST targets miR-340-5p. (A) Binding sites between XIST and miR-340-5p were predicted by StarBase; (B) binding relationship between XIST and miR-340-5p was confirmed by dual luciferase reporter gene assay; (C) binding relationship between XIST and miR-340-5p was verified by RNA pull-down assay; (D and E) miR-340-5p expression in mice detected by RT-qPCR; $N = 3$ in (A)–(C), $n = 6$ in (D) and (E); $^{*}P < 0.05$ versus the sham group, $^{\#}P < 0.05$ versus the NC group; the data were expressed as mean ± standard deviation, and the *t*-test was performed for comparisons between two groups.

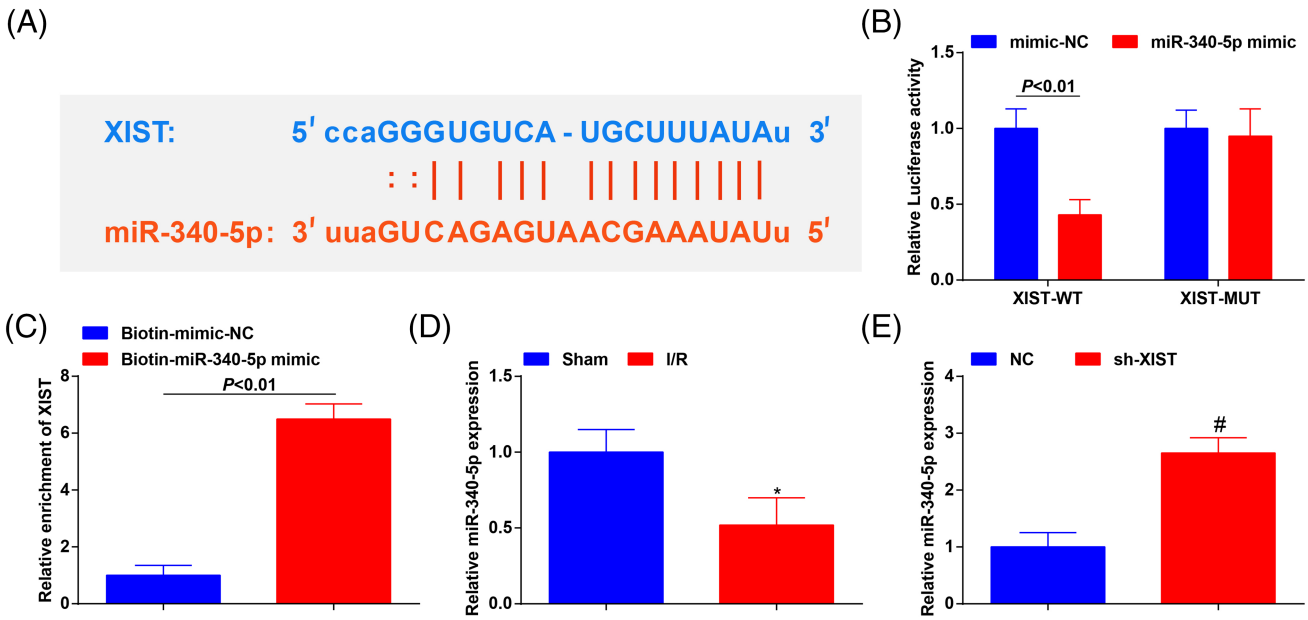

DOI: 10.1002/ehf2.13766

Figure 4 MiR-340-5p reduction aggravates XIST-induced MIRI. (A) miR-340-5p expression in mice detected by RT-qPCR; (B) detection of myocardial enzyme activity; (C–E) detection of cardiac blood flow parameters; (F) representative images of HE staining; (G) representative images of Masson staining; (H) representative images of TUNEL staining; (I) mRNA expression of Bcl-2, Bax, and Caspase-3 assessed by RT-qPCR; (J–M) detection of oxidative stress-related factor levels; (N) levels of inflammatory factors; $n = 12$ in (B)–(E), $n = 6$ in (A), (F)–(N); $^{+}P < 0.05$ versus the antagomir NC group, $^{\$}P < 0.05$ versus the miR-340-5p antagomir group; the data were expressed as mean ± standard deviation, ANOVA was used for comparisons among multiple groups, and Tukey's post hoc test was used for pairwise comparisons after ANOVA.

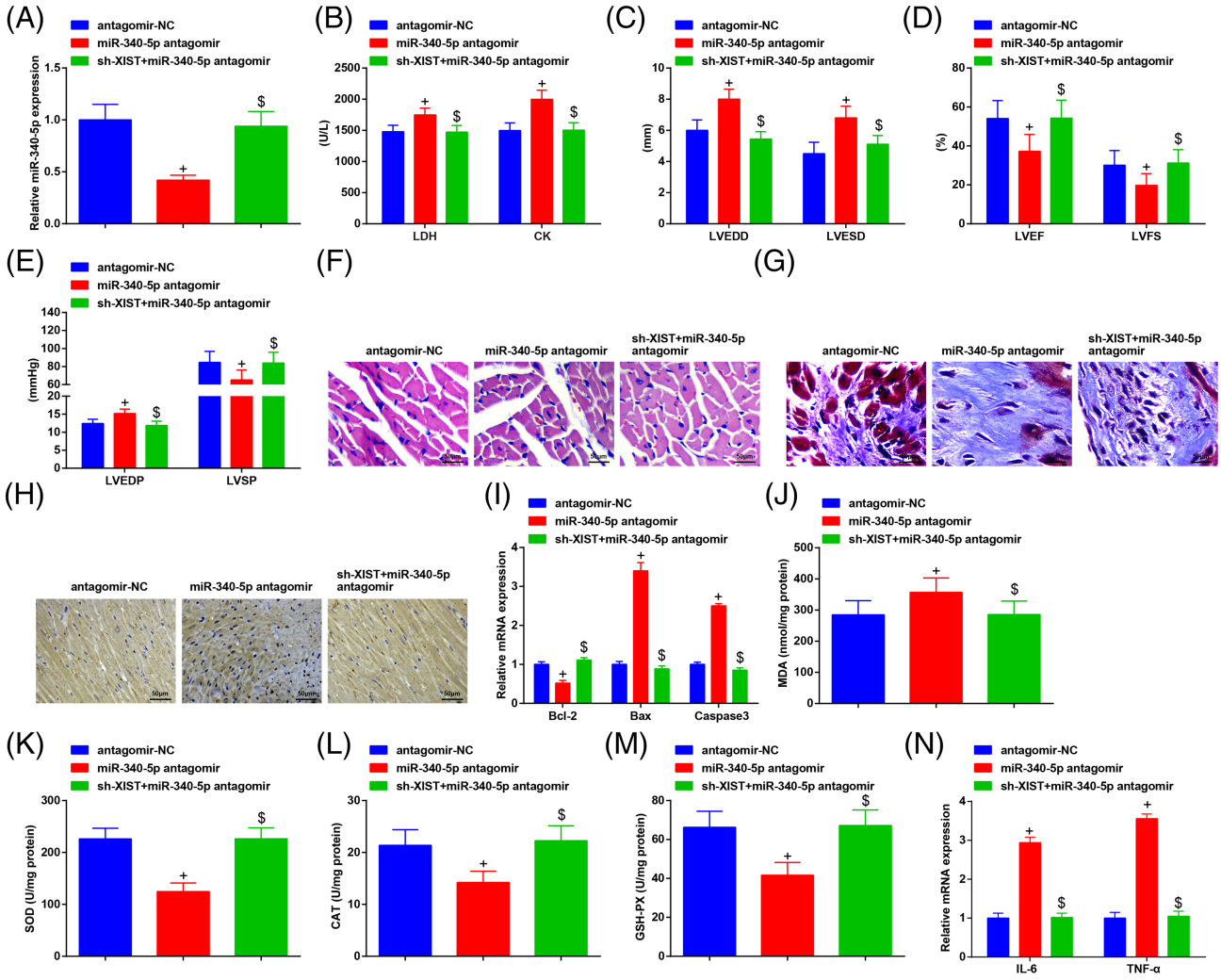

promoted cardiac function in the I/R mice; the knockdown of XIST and miR-340-5p restored the levels of cardiac parameters to that in antagomir NC group in mice (*Figure 4B–4N*). The aforementioned data mirrored that miR-340-5p functioned in the downstream of XIST-induced MIRI regulatory axis.

MiR-340-5p targets cyclin D1

The binding sites between miR-340-5p and CCND1 were predicted (*Figure 5A*), and it was further confirmed that the co-transfection of miR-340-5p mimic and CCND1-WT inhibited the luciferase activity while that of miR-340-5p mimic and CCND1-MUT did not affect the luciferase activity (*Figure 5B*), indicating a direct interaction between miR-340-5p and CCND1. Furthermore, results of RT-qPCR and Western blot analysis reflected that CCND1 was up-regulated in I/R mice and its expression was negatively regulated by miR-340-5p (*Figure 5C–5E*). These findings suggested that CCND1 was a target gene of miR-340-5p.

Cyclin D1 inhibition attenuates myocardial ischaemia–reperfusion injury

MiR-340-5p was down-regulated to observe the impact of the functional axis of XIST, and we also found through

Figure 5 MiR-340-5p targets CCND1. (A) RNA22 was used to predict the binding sites of miR-340-5p and CCND1; (B) targeting relationship between miR-340-5p and CCND1 was confirmed by dual luciferase reporter gene assay; (C) CCND1 expression in sham and I/R mice; (D/E) mRNA and protein expression of CCND1 in I/R mice treated with miR-340-5p antagomir was determined using RT-qPCR and Western blot analysis; $N = 3$ in (A) and (B), $n = 6$ in (C)–(E); $^{*}P < 0.05$ versus the sham group, $^{+}P < 0.05$ versus the antagomir NC group; the data were expressed as mean ± standard deviation, and the *t*-test was performed for comparisons between two groups.

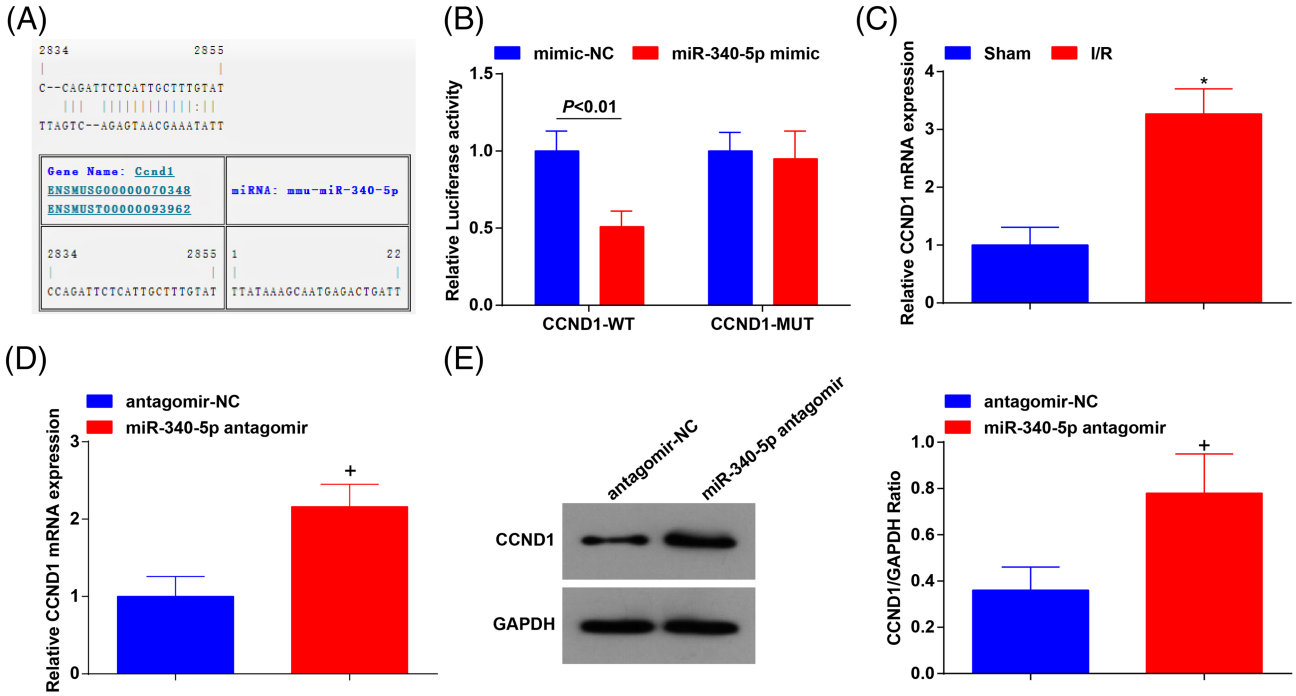

RT-qPCR and Western blot analysis that si-XIST down-regulated CCND1 (*Figure 6A–6C*). The outcomes of our experiments mirrored that the inhibition of CCND1 restrained myocardial enzyme activity, pathological changes, cardiomyocyte apoptosis, oxidative stress, and inflammatory response and improved cardiac function in the I/R mice (*Figure 6D–6P*). It can be concluded that XIST suppression ameliorated MIRI via targeting the miR-340-5p/CCND1 axis.

Discussion

While reperfusion is the main treatment of myocardial ischaemia in the setting of coronary occlusion, it can lead to serious myocardial damage through MIRI.[26] We aimed to explore the effect of the XIST/miR-340-5p/CCND1 axis on the development of MIRI, and we found that XIST inhibition could up-regulate miR-340-5p to protect against the MIRI via reducing CCND1.

We assessed the expression of XIST in mouse myocardial tissues and found that the MIRI mice had higher XIST expression in comparison with the sham-operated ones. In line with this finding, a recent publication has indicated that XIST is overexpressed in both H/R H9C2 cells and I/R mouse myocardial tissues,[12] and Zhou *et al*. have clarified that the expression of XIST is increased in post-MI myocardial cells.[10] XIST was knocked down to figure out its role in the progression of MIRI, and the results of a series assays implied that the reduction of XIST promoted cardiac function and suppressed myocardial enzyme activity, ischaemia area, cardiomyocyte apoptosis, inflammatory response, and oxidative stress in MIRI mice. Consistent with our outcomes, it has been revealed that XIST silencing represses apoptosis of hypoxic cardiomyocytes *in vitro* and inhibits MI in a mouse model by regulating apoptosis-related proteins,[27] Wang *et al*. have found that down-regulated XIST restrains inflammatory response in diabetic nephropathy,[28] and decreased XIST expression has also been reported to attenuate oxidative stress and apoptosis in primary cultured rat hippocampal neurons.[29] In addition, lncRNAs are known to serve as ceRNAs to sponge the miRNAs, and XIST has been identified to sponge miR-125b in hypoxia-induced cardiomyocyte injury[30] and miR-133 in MIRI,[12] while the binding between XIST and miR-340-5p still needs to be further explored.

MiR-340-5p expression was determined as well, and we found that it was down-regulated in myocardial tissues from MIRI mice. Consistently, Li *et al*. have unveiled that miR-340-5p was down-regulated after I/R in MI mice and H/R-induced cardiomyocytes,[15] and it has been reported that miR-340-5p

Figure 6 CCND1 inhibition attenuates MIRI. (A) CCND1 expression in I/R mice treated with sh-CCND1; (B/C) mRNA and protein expression of CCND1 in mice treated with sh-XIST; (D) detection of myocardial enzyme activity; (E–G) detection of cardiac blood flow parameters; (H) representative images of HE staining; (I) representative images of Masson staining; (J) representative images of TUNEL staining; (K) mRNA expression of Bcl-2, Bax, and Caspase-3 assessed by RT-qPCR; (L–O) detection of oxidative stress-related factor levels; (P) levels of inflammatory factors; n = 12 in (D)–(G), n = 6 in (A)–(C), (H)–(P); $^{\#}P < 0.05$ versus the NC group; the data were expressed as mean ± standard deviation, and the t-test was performed for comparisons between two groups.

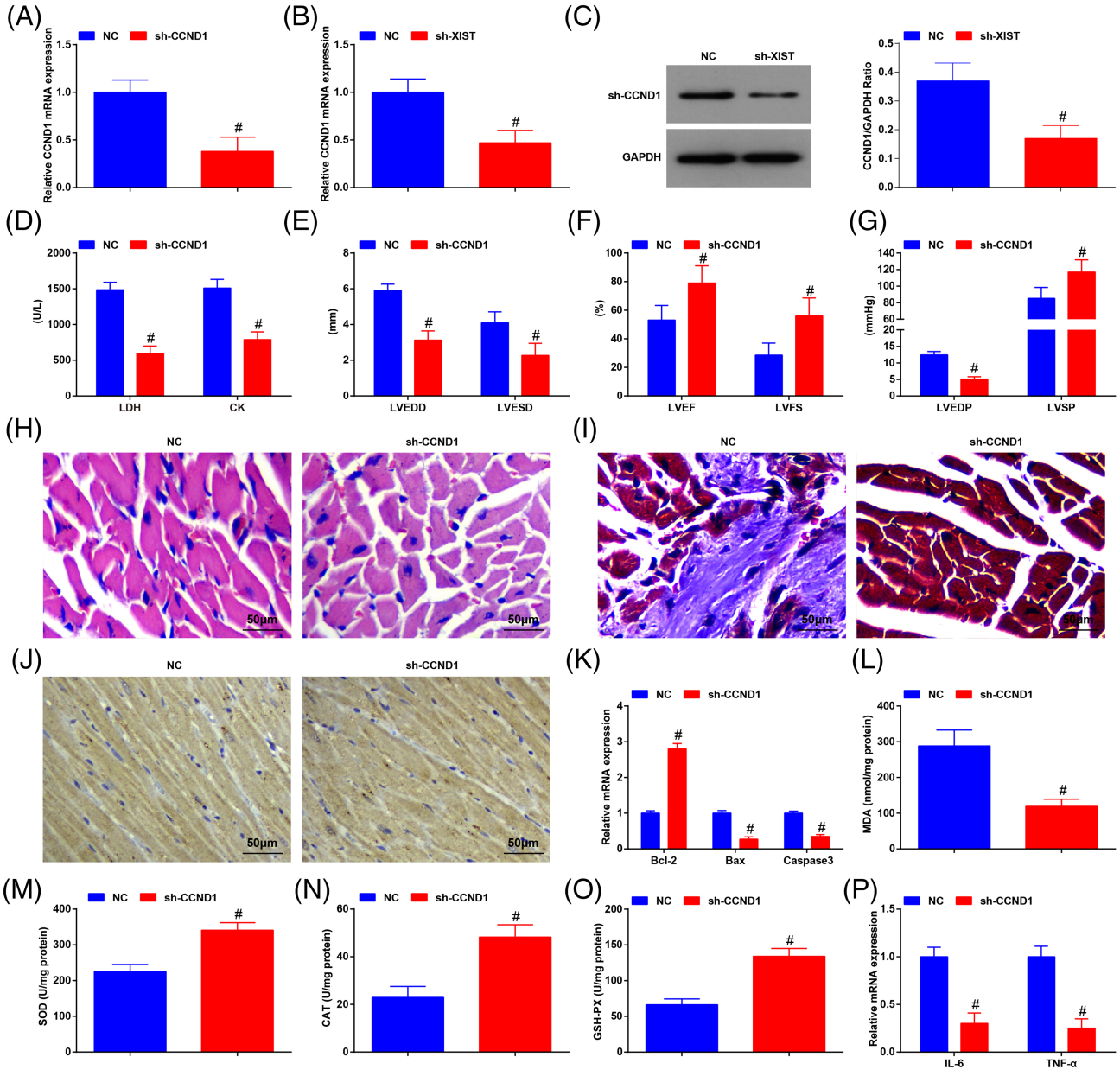

is poorly expressed in oxygen–glucose deprivation/reoxygenation (OGDR)-stimulated neurons.[31] The expression of miR-340-5p was altered as well to investigate its impact on MIRI, and we discovered that miR-340-5p down-regulation impaired cardiac function and promoted myocardial enzyme activity, ischaemia area, cardiomyocyte apoptosis, inflammatory response, and oxidative stress in MIRI mice. Similarly, it has been clarified that miR-340-5p restricts H/R-induced apoptosis and oxidative stress in cardiomyocytes,[15] and Qian *et al*. have elucidated that the up-regulation of miR-340-5p ameliorates spinal cord injury-induced neuroinflammation and apoptosis.[32] In addition, Zheng *et al*. have illustrated that miR-340-5p alleviates OGDR-induced neuronal injury.[31] Moreover, we confirmed using bioinformatic predic-

tion and dual luciferase reporter gene assay that miR-340-5p targeted CCND1 in MIRI. In accordance with our finding, it has been reported that there exists a targeting relationship between miR-340-5p and CCND1 in multiple myeloma.[18] CCND1 expression was also assessed and it was revealed that in rats underwent I/R and partial hepatectomy injury, CCND1 showed an increased expression level in transplanted grafts with macrosteatosis.[33] Additionally, we found through the gain-of-function and loss-of-function assays that CCND1 inhibition could relieve the MIRI. Similar to our result, Pei *et al*. have identified that the down-regulation of CCND1 protects against cerebral ischaemia in a middle cerebral artery occlusion model.[34]

In conclusion, we discovered that the silencing of XIST upregulates miR-340-5p to alleviate the MIRI in a mouse model through inhibiting CCND1. This study may provide novel biomarkers for MIRI treatment. However, the study sample can be further expanded in future studies to diminish the data errors in experimental results.

Conflict of interest

The authors have no conflicts of interest to declare that are relevant to the content of this article.

Supporting information

Additional supporting information may be found online in the Supporting Information section at the end of the article.

Table S1. Primer sequence used for q-PCR.

References

1. Mokhtari-Zaer A, Marefati N, Atkin SL, Butler AE, Sahebkar A. The protective role of curcumin in myocardial ischemia-reperfusion injury. *J Cell Physiol* 2018; **234**: 214–222.
2. Ali M, Girgis S, Hassan A, Rudick S, Becker RC. Inflammation and coronary artery disease: from pathophysiology to Canakinumab Anti-Inflammatory Thrombosis Outcomes Study (CANTOS). *Coron Artery Dis* 2018; **29**: 429–437.
3. Huang ZQ, Xu W, Wu JL, Lu X, Chen XM. MicroRNA-374a protects against myocardial ischemia-reperfusion injury in mice by targeting the MAPK6 pathway. *Life Sci* 2019; **232**: 116619.
4. Xie B, Liu X, Yang J, Cheng J, Gu J, Xue S. PIAS1 protects against myocardial ischemia-reperfusion injury by stimulating PPARγ SUMOylation. *BMC Cell Biol* 2018; **19**: 24.
5. Hausenloy DJ, Yellon DM. Myocardial ischemia-reperfusion injury: a neglected therapeutic target. *J Clin Invest* 2013; **123**: 92–100.
6. Wang Y, Gong G, Xu J, Zhang Y, Wu S, Wang S. Long noncoding RNA HOTAIR promotes breast cancer development by targeting ZEB1 via sponging miR-601. *Cancer Cell Int* 2020; **20**: 320.
7. Kong F, Jin J, Lv X, Han Y, Liang X, Gao Y, Duan X. Long noncoding RNA RMRP upregulation aggravates myocardial ischemia-reperfusion injury by sponging miR-206 to target ATG3 expression. *Biomed Pharmacother* 2019; **109**: 716–725.
8. Yu SY, Dong B, Fang ZF, Hu XQ, Tang L, Zhou SH. Knockdown of lncRNA AK139328 alleviates myocardial ischaemia/reperfusion injury in diabetic mice via modulating miR-204-3p and inhibiting autophagy. *J Cell Mol Med* 2018; **22**: 4886–4898.
9. Rong H, Chen B, Wei X, Peng J, Ma K, Duan S, He J. Long non-coding RNA XIST expedites lung adenocarcinoma progression through upregulating MDM2 expression via binding to miR-363-3p. *Thorac Cancer* 2020; **11**: 659–671.
10. Zhou T, Qin G, Yang L, Xiang D, Li S. LncRNA XIST regulates myocardial infarction by targeting miR-130a-3p. *J Cell Physiol* 2019; **234**: 8659–8667.
11. Zhang M, Liu HY, Han YL, Wang L, Zhai DD, Ma T, Zhang MJ, Liang CZ, Shen Y. Silence of lncRNA XIST represses myocardial cell apoptosis in rats with acute myocardial infarction through regulating miR-449. *Eur Rev Med Pharmacol Sci* 2019; **23**: 8566–8572.
12. Li Z, Zhang Y, Ding N, Zhao Y, Ye Z, Shen L, Yi H, Zhu Y. Inhibition of lncRNA XIST improves myocardial I/R injury by targeting miR-133a through inhibition of autophagy and regulation of SOCS2. *Mol Ther Nucleic Acids* 2019; **18**: 764–773.
13. Tan X, Wang P, Lou J, Zhao J. Knockdown of lncRNA NEAT1 suppresses hypoxia-induced migration, invasion and glycolysis in anaplastic thyroid carcinoma cells through regulation of miR-206 and miR-599. *Cancer Cell Int* 2020; **20**: 132.
14. Khalaj M, Woolthuis CM, Hu W, Durham BH, Chu SH, Qamar S, Armstrong SA, Park CY. miR-99 regulates normal and malignant hematopoietic stem cell self-renewal. *J Exp Med* 2017; **214**: 2453–2470.
15. Li D, Zhou J, Yang B, Yu Y. microRNA-340-5p inhibits hypoxia/reoxygenation-induced apoptosis and oxidative stress in cardiomyocytes by regulating the Act1/NF-κB pathway. *J Cell Biochem* 2019; **120**: 14618–14627.
16. Zang Y, Li J, Wan B, Tai Y. circRNA circ-CCND1 promotes the proliferation of laryngeal squamous cell carcinoma through elevating CCND1 expression via interacting with HuR and miR-646. *J Cell Mol Med* 2020; **24**: 2423–2433.
17. Liu L, Li J, Wang R, Wang Y, Wang G. MicroRNA-298 exacerbates myocardial ischemic injury via targeting cyclin D1. *Pharmazie* 2019; **74**: 369–373.
18. Li Z, Wong KY, Calin GA, Chng WJ, Chan GCF, Chim CS. Epigenetic silencing of miR-340-5p in multiple myeloma: mechanisms and prognostic impact. *Clin Epigenetics* 2019; **11**: 71.
19. Song YF, Zhao L, Wang BC, Sun JJ, Hu JL, Zhu XL, Zhao J, Zheng DK, Ge ZW. The circular RNA TLK1 exacerbates myocardial ischemia/reperfusion injury via targeting miR-214/RIPK1 through TNF signaling pathway. *Free Radic Biol Med* 2020; **155**: 69–80.
20. Tang P, Ma S, Dong M, Wang J, Chai S, Liu T, Li J. Effect of interleukin-6 on myocardial regeneration in mice after cardiac injury. *Biomed Pharmacother* 2018; **106**: 303–308.
21. Yang M, Chen J, Zhao J, Meng M. Etanercept attenuates myocardial ischemia/reperfusion injury by decreasing inflammation and oxidative stress. *PLoS ONE* 2014; **9**: e108024.
22. Fang HC, Wu BQ, Hao YL, Luo Y, Zhao HL, Zhang WY, Zhang ZL, Liang JJ, Liu W, Chen XH. KRT1 gene silencing ame-

liorates myocardial ischemia-reperfusion injury via the activation of the Notch signaling pathway in mouse models. *J Cell Physiol* 2019; **234**: 3634–3646.
23. Wang R, Yang M, Wang M, Liu X, Xu H, Xu X, Sun G, Sun X. Total saponins of *Aralia elata* (Miq) seem alleviate calcium homeostasis imbalance and endoplasmic reticulum stress-related apoptosis induced by myocardial ischemia/reperfusion injury. *Cell Physiol Biochem* 2018; **50**: 28–40.
24. Pan S, Chen Y, Zhang X, Xie Y. The JAK2/STAT3 pathway is involved in dexmedetomidine-induced myocardial protection in rats undergoing cardiopulmonary bypass. *Ann Transl Med* 2020; **8**: 483.
25. Xu Y, Tang C, Tan S, Duan J, Tian H, Yang Y. Cardioprotective effect of isorhamnetin against myocardial ischemia reperfusion (I/R) injury in isolated rat heart through attenuation of apoptosis. *J Cell Mol Med* 2020; **24**: 6253–6262.
26. Li J, Zhao Y, Zhou N, Li L, Li K. Dexmedetomidine attenuates myocardial ischemia-reperfusion injury in diabetes mellitus by inhibiting endoplasmic reticulum stress. *J Diabetes Res* 2019; **2019**: 7869318.
27. Lin B, Xu J, Wang F, Wang J, Zhao H, Feng D. LncRNA XIST promotes myocardial infarction by regulating FOS through targeting miR-101a-3p. *Aging (Albany NY)* 2020; **12**: 7232–7247.
28. Wang Q. XIST silencing alleviated inflammation and mesangial cells proliferation in diabetic nephropathy by sponging miR-485. *Arch Physiol Biochem* 2020: 1–7.
29. Wang X, Wang C, Geng C, Zhao K. LncRNA XIST knockdown attenuates Aβ25-35-induced toxicity, oxidative stress, and apoptosis in primary cultured rat hippocampal neurons by targeting miR-132. *Int J Clin Exp Pathol* 2018; **11**: 3915–3924.
30. Fan JL, Zhu TT, Xue ZY, Ren WQ, Guo JQ, Zhao HY, Zhang SL. lncRNA-XIST protects the hypoxia-induced cardiomyocyte injury through regulating the miR-125b-hexokianse 2 axis. *In Vitro Cell Dev Biol Anim* 2020; **56**: 349–357.
31. Zheng Y, Zhao P, Lian Y, Li S, Chen Y, Li L. MiR-340-5p alleviates oxygen-glucose deprivation/reoxygenation-induced neuronal injury via PI3K/Akt activation by targeting PDCD4. *Neurochem Int* 2020; **134**: 104650.
32. Qian Z, Chang J, Jiang F, Ge D, Yang L, Li Y, Chen H, Cao X. Excess administration of miR-340-5p ameliorates spinal cord injury-induced neuroinflammation and apoptosis by modulating the P38-MAPK signaling pathway. *Brain Behav Immun* 2020; **87**: 531–542.
33. Nunez KG, Frank A, Gonzalez-Rosario J, Galliano G, Bridle K, Crawford D, Seal J, Abbruscato F, Vashistha H, Thevenot PT, Cohen AJ. Interleukin-33/Cyclin D1 imbalance in severe liver steatosis predicts susceptibility to ischemia reperfusion injury. *PLoS ONE* 2019; **14**: e0216242.
34. Pei L, Zhang Y, Zhang Y, Chu X, Zhang J, Wang R, Liu M, Zhu X, Yu W. Peroxisome proliferator-activated receptor gamma promotes neuroprotection by modulating cyclin D1 expression after focal cerebral ischemia. *Can J Physiol Pharmacol* 2010; **88**: 716–723.